

NASA Technical Memorandum 105327

1N-07
53179

(NASA-TM-105327) DEVELOPMENT OF A COMPUTER
ALGORITHM FOR THE ANALYSIS OF
VARIABLE-FREQUENCY AC DRIVES: CASE STUDIES
INCLUDED (NASA) 34 D CSCL 21F

N92-13070

Unclas
63/07 0053179

Development of a Computer Algorithm for the Analysis of Variable-Frequency A.C. Drives – Case Studies Included

M. David Kankam
Lewis Research Center
Cleveland, Ohio

and

Owen Benjamin
Cornell University
Ithaca, New York

November 1991

NASA



TABLE OF CONTENTS

| | |
|---|-----------|
| <u>Abstract</u> | 1 |
| <u>I. Introduction</u> | 1 |
| <u>II. Modeling of Drive Sources</u> | 2 |
| II.1 Pulse Width Modulated Inverter | 2 |
| II.2 Six-Step Inverter | 5 |
| II.3 Pulse Density Modulated Inverter | 6 |
| <u>III. Induction Machine Modeling</u> | 8 |
| III.1 Basic Machine Equations | 8 |
| III.2 Transformation to d-q Variables | 10 |
| III.3 Reference Frames | 11 |
| III.3.1 Arbitrary Reference Frame | 11 |
| III.3.2 Synchronous Rotating Reference Frame | 11 |
| III.3.3 Multiple Reference Frame | 12 |
| III.4 Derivation of Multiple Reference Frame Voltages | 13 |
| <u>IV. Simulation Results</u> | 16 |
| IV.1 Parameters of Induction Machine | 16 |
| IV.2 6-Step Inverter Induction Machine Drive | 17 |
| IV.3 PWMI - Induction Machine Drive | 22 |
| IV.4 PDMI - Induction Machine Drive | 24 |
| <u>V. Summary</u> | 26 |
| <u>References</u> | 27 |
| <u>Appendices</u> | |
| A1. Flow Charts | 28 |

Development of a Computer Algorithm for the Analysis of Variable-Frequency A.C. Drives - Case Studies Included

M. David Kankam

National Aeronautics and Space Administration
Lewis Research Center
Cleveland, Ohio 44135

and

Owen Benjamin*

Cornell University
Ithaca, New York 14850

ABSTRACT

This report documents the development of a computer software for performance prediction and analysis of voltage-fed, variable-frequency AC drives for space power applications. The AC drives discussed include the pulse width modulated inverter (PWMI), the six-step inverter and the pulse density modulated inverter (PDMI), each individually connected to a wound-rotor induction motor. Various d-q transformation models of the induction motor are incorporated for user-selection of the most applicable model for the intended purpose.

Simulation results of selected AC drives correlate satisfactorily with published results. Future additions to the algorithm are indicated in the Summary. These improvements should enhance the applicability of the computer program to the design and analysis of space power systems.

I. INTRODUCTION

Variable-frequency drives have been extensively documented in the literature. Most publications deal with a particular problem area and application. In the realm of space mission applications, there is a need to incorporate flexibility for options and assessment on various potential voltage-fed inverters as possible drive sources for selected A.C. machinery.

This report describes the development of a computer algorithm for performance prediction and the analysis of variable-frequency A.C. drives. These drives have a potential application in space missions. Among the AC drives discussed are the pulsewidth modulated inverter(PWMI), the six-step inverter and the pulse density modulated inverter(PDMI). A general synthesis of the PWMI output is described. The outputs of the inverters are d-q transformed for subsequent excitation of a similarly transformed, symmetrical induction machine model. The algorithm accommodates transformation in the arbitrary, fixed, synchronously rotating and multiple reference frames of operation. A complete flow-chart of the algorithm is provided in the Appendix.

Simulation results obtained by the algorithm are compared with pertinent publication for verification. Salient characteristics of the results are discussed. Included in the summary are planned additions for subsequent incorporation in the algorithm. These extensions should further improve the usefulness of the algorithm for studies relating to space power applications.

*1991 Summer OAI/NASA Collaborative Aerospace Intern at Lewis Research Center.

II. MODELING OF DRIVE SOURCES

This section discusses various AC drives individually applied to a three-phase symmetrical induction machine. These drives permit a comparison of the effects of their output harmonic content on the performance characteristics of the induction machine. Also, the use of these drives demonstrates the flexibility of the developed algorithm in its choice of a particular drive for the intended application.

II.1 Pulse Width Modulated Inverter (PWMI)

A Pulse Width Modulated Inverter has been simulated from development of an analytical procedure for deriving input harmonic voltages applicable to a variable frequency AC drive. The synthesis for obtaining an analytical expression for the line-to-line synchronized voltage waveform, $v_{L-L}(t)$, from a line-to-line voltage envelope, $v_e(t)$, and a continuous pulse operator, $v_p(t)$, is shown schematically in Fig. II-1. A summary of the method follows. The complete modeling details of the PWMI is contained in a NASA-Lewis 1990 Summer Report.[1]

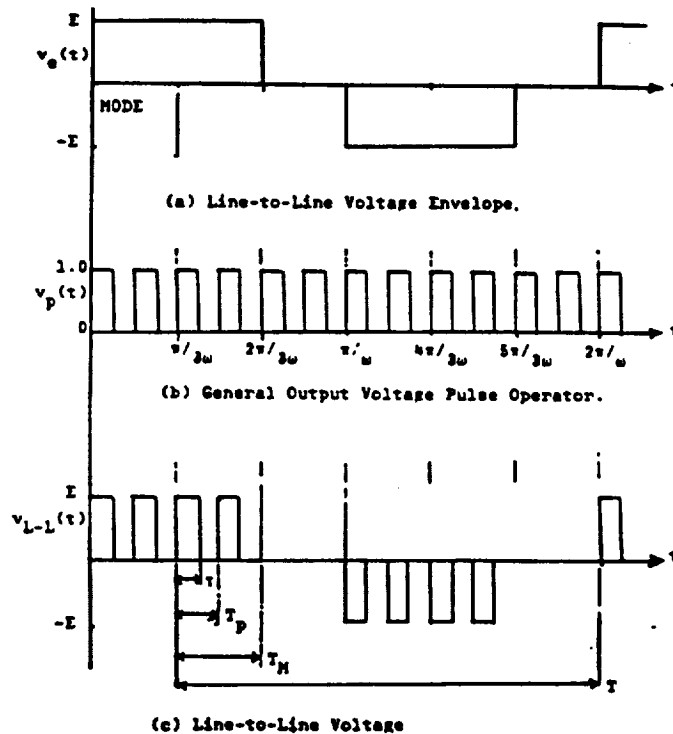


Fig. II-1 - Synthesis of Line-to-Line Synchronized Voltage Waveform

The voltage envelope controls the output frequency of the synchronized waveform, while the voltage pulse operator controls the number of pulses within a half cycle and the duration of time the switches stay closed.

Reference [2] shows that the general synchronized voltage waveform, in Fig. II-1, has the

following constraints:

$$\begin{aligned} \omega_p / \omega &\geq 6 \\ 0 \leq \tau / T_p &\leq 1 \\ dE / dt &= 0 \end{aligned} \tag{1}$$

where,

- E = amplitude (d.c. volts) of the line-line voltage envelope $v_e(t)$;
- $\omega = 2\pi/\tau$ = fundamental frequency of the output voltage (rad/s) of the inverter;
- $\omega_p = 2\pi/T_p$ = multi-pulse frequency (rad/s)
 - = time interval between leading edges of two consecutive pulses of the voltage operator $v_p(t)$.
- τ = pulse width (secs) of $v_p(t)$.
- T_M = mode period (secs) = $T/6$.

The synthesized line-to-line output waveform of the PWMI is obtained from the relation:

$$v_{L-L}(t) = v_e(t) * v_p(t) \tag{2}$$

The voltage operator is defined in eqn. (3),

$$v_p(t) = \begin{cases} g_p(t) & , & 0 \leq t \leq \pi/3\omega \\ g_p(t - \pi/3\omega) & , & \pi/3\omega \leq t \leq 2\pi/3\omega \\ g_p(t - 2\pi/3\omega) & , & 2\pi/3\omega \leq t \leq \pi/\omega \end{cases} \tag{3}$$

The Fourier expression for the unity amplitude multipulse operator is stated in eqn. (4).

$$g_p(t) = \frac{\tau}{T_p} + \sum_n \frac{\sqrt{2}}{n\pi} \sqrt{1 - \cos n\omega_p \tau} \cdot \sin(n\omega_p t + \eta)$$

$$\eta = \tan^{-1} \left(\frac{\sin n\omega_p \tau}{1 - \cos n\omega_p \tau} \right) \quad (4)$$

$$n = 1, 2, 3, 4, \dots$$

Equation (5) shows the general Fourier expression of the line-to-line voltage

$$v_{L-L}(t) = \sum_k a_k \cos k\omega t + b_k \sin k\omega t, \quad k=1, 5, 7, \dots \quad (5)$$

where the coefficients are

$$a_k = \frac{E}{\pi} \left[\frac{2\tau}{kT_p} \cdot \sin \frac{2\pi k}{3} + \frac{\sum_{n=1}^{\infty} F_n \left(\frac{3n\omega_p}{\omega} \cdot \cos \eta + 2k \sin \frac{\pi k}{3} \cdot (G_n) \right)}{H_n} \right] \quad (6)$$

$$b_k = \frac{E}{\pi} \left[\frac{3\tau}{kT_p} + \frac{\sum_{n=1}^{\infty} F_n \left(\frac{2n\omega_p}{\omega} \cdot \sin \frac{\pi k}{3} \cdot (J_n) - 3k \sin \eta \right)}{H_n} \right]$$

Other variables in eqn. (6) are given in eqn. (7).

$$F_n = \frac{\sqrt{2}}{n\pi} \sqrt{1 - \cos n\omega_p \tau} \quad (7)$$

$$H_n = \left(\frac{n\omega_p}{\omega} \right)^2 - k^2$$

$$G_n = -2 \sin \left(\frac{n\pi\omega_p}{3\omega} + \eta \right) + \sin \eta$$

$$J_n = -2 \cos \left(\frac{n\pi\omega_p}{3\omega} + \eta \right) + \cos \eta$$

$$k = 1, 5, 7, 11, 13, \dots$$

Typical values used in subsequent simulation are summarized below.

$$E = 115\text{v D.C}$$

$$\omega = \text{operating frequency}$$

$$= 12 \text{ Hz, } 30 \text{ Hz, } 54 \text{ Hz}$$

$$\omega_{eb} = \text{base frequency (rated)}$$

$$= 60 \text{ Hz}$$

$$\omega_p = 360 \text{ Hz}$$

$$\tau = \frac{\omega}{\omega_{eb}} T_p$$

$$V_{\text{base}} = \text{line-to-neutral r.m.s voltage at } \omega = \omega_{eb}$$

$$= 51.77 \text{ v}$$

II.2. Six-Step Inverter

Figure II-2a shows a schematic for the basic circuit of a six-step inverter induction motor drive. Typically, the control of the magnitude of the dc link voltage, V_I , is achieved by maintaining a constant v/f ratio.

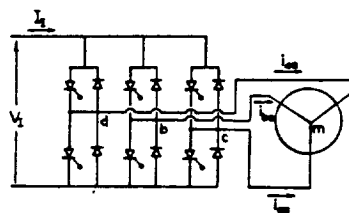


Fig. II-2a - Inverter-Induction Motor Drive

The six-step inverter is designed so that the output separates in six distinct 60 degree periods in one cycle. This form of output is sometimes referred to as the "staircase" waveform, depicted in Fig. II-2b for one phase voltage of the inverter.[3]

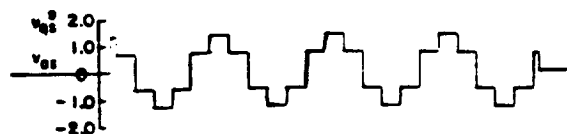


Fig. II-2b - Output Voltage Waveform of a Six-Step Inverter

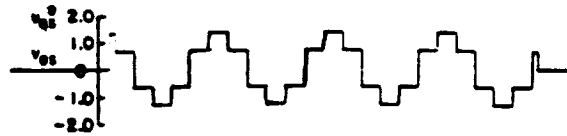


Fig. II-2b - Output Voltage Waveform of a Six-Step Inverter

II.3 Pulse Density Modulated Inverter (PDMI)

Analysis of the output of the Pulse Density Modulated Inverter is based on a synthesized waveform in reference[5] and shown in Fig. II-3. Using a constraint of zero voltage switching, a low frequency voltage component, v_{LF} , is derived from complete half cycles of the high - frequency link voltage, v_{HF} .

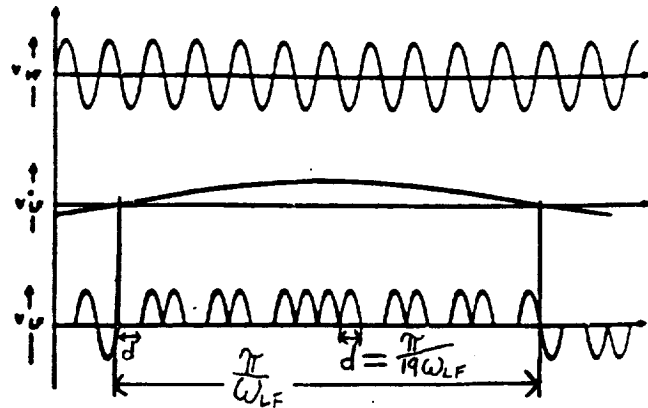


Fig. II-3 - PDM Synthesis of low-frequency Voltage

The third waveform, v_{LF} , displayed in Fig. II-3 is the output synthesized from the first two input wave signals. This waveform may be Fourier analyzed and applied to a connected AC machine. This is achieved by either a programmed logic or some form of a modulation scheme. Fourier analysis of the this particular frequency output is shown below.

$$v_{LF}(t) = \sum \{ a_k * \sin(k * \omega t) + b_k * \cos(k * \omega t) \},$$

where

$$\begin{aligned}
a_k = (2 * E_m * \omega_{Lf}) / \pi * \\
& \left\{ \int_{d}^{2d} -f_c(t) dt + \int_{2d}^{3d} f_c(t) dt + \int_{4d}^{5d} f_c(t) dt + \int_{5d}^{6d} -f_c(t) dt + \int_{7d}^{8d} -f_c(t) dt + \right. \\
& \int_{8d}^{9d} f_c(t) dt + \int_{9d}^{10d} -f_c(t) dt + \int_{10d}^{11d} f_c(t) dt + \int_{12d}^{13d} f_c(t) dt + \int_{13d}^{14d} -f_c(t) dt + \\
& \left. \int_{15d}^{16d} -f_c(t) dt + \int_{16d}^{17d} f_c(t) dt + \int_{18d}^{19d} f_c(t) dt \right\}
\end{aligned} \tag{8}$$

and

$$f_c(t) = \sin(\omega_{Hf} * t) * \cos(k * \omega_{Lf} * t),$$

$$d = \pi / (19 * \omega_{Lf}).$$

Expansion and simplification of eqn. (8) results in the expression of eqn. (9).

$$\begin{aligned}
a_k = [E_m * \omega_{Lf} / \pi] * \{ [(-\cos(d * \alpha) - \cos(3 * d * \alpha) + \cos(4 * d * \alpha) + \cos(6 * d * \alpha) - \cos(7 * d * \alpha) - \\
\cos(11 * d * \alpha) + \cos(12 * d * \alpha) + \cos(14 * d * \alpha) - \cos(15 * d * \alpha) - \\
\cos(17 * d * \alpha) + \cos(18 * d * \alpha) - \cos(19 * d * \alpha) + 2 * \cos(2 * d * \alpha) - \\
2 * \cos(5 * d * \alpha) + 2 * \cos(8 * d * \alpha) - 2 * \cos(9 * d * \alpha) + \\
2 * \cos(10 * d * \alpha) - 2 * \cos(13 * d * \alpha) + 2 * \cos(16 * d * \alpha)) / \alpha] + \\
[(-\cos(d * \beta) - \cos(3 * d * \beta) + \cos(4 * d * \beta) + \cos(6 * d * \beta) - \cos(7 * d * \beta) - \\
\cos(11 * d * \beta) + \cos(12 * d * \beta) + \cos(14 * d * \beta) - \cos(15 * d * \beta) - \\
\cos(17 * d * \beta) + \cos(18 * d * \beta) - \cos(19 * d * \beta) + 2 * \cos(2 * d * \beta) - \\
2 * \cos(5 * d * \beta) + 2 * \cos(8 * d * \beta) - 2 * \cos(9 * d * \beta) + \\
2 * \cos(10 * d * \beta) - 2 * \cos(13 * d * \beta) + 2 * \cos(16 * d * \beta)) / \beta] \},
\end{aligned} \tag{9}$$

where

$$\alpha = \omega_{Hf} + (k * \omega_{Lf})$$

$$\beta = \omega_{Hf} - (k * \omega_{Lf}).$$

A similar derivation holds for b_k if

$$f_s(t) = \sin(\omega_{Hf} * t) * \sin(k * \omega_{Lf} * t) \quad (10)$$

is substituted for $f_c(t)$ in eqn. (8). This yields the expression of eqn. (11).

$$b_k = [E_m * \omega_{Lf} / \pi] * \{ [(-\sin(d * \alpha) - \sin(3 * d * \alpha) + \sin(4 * d * \alpha) + \sin(6 * d * \alpha) - \sin(7 * d * \alpha) - \sin(11 * d * \alpha) + \sin(12 * d * \alpha) + \sin(14 * d * \alpha) - \sin(15 * d * \alpha) - \sin(17 * d * \alpha) + \sin(18 * d * \alpha) - \sin(19 * d * \alpha) + 2 * \sin(2 * d * \alpha) - 2 * \sin(5 * d * \alpha) + 2 * \sin(8 * d * \alpha) - 2 * \sin(9 * d * \alpha) + 2 * \sin(10 * d * \alpha) - 2 * \sin(13 * d * \alpha) + 2 * \sin(16 * d * \alpha)) / \alpha] + [(\sin(d * \beta) + \sin(3 * d * \beta) - \sin(4 * d * \beta) - \sin(6 * d * \beta) + \sin(7 * d * \beta) + \sin(11 * d * \beta) - \sin(12 * d * \beta) - \sin(14 * d * \beta) + \sin(15 * d * \beta) + \sin(17 * d * \beta) - \sin(18 * d * \beta) + \sin(19 * d * \beta) - 2 * \sin(2 * d * \beta) + 2 * \sin(5 * d * \beta) - 2 * \sin(8 * d * \beta) + 2 * \sin(9 * d * \beta) - 2 * \sin(10 * d * \beta) + 2 * \sin(13 * d * \beta) - 2 * \sin(16 * d * \beta)) / \beta] \} \quad (11)$$

Each of the above voltage sources is subsequently used as a driving source to simulate the performance of a wound-rotor induction motor.

III. INDUCTION MACHINE MODELING

This section describes the derivation of the d-q transformation model of an induction machine. Various forms of the model are discussed for the arbitrary, synchronous rotating and the multiple reference frames.

III.1 Basic Machine Equations

A schematic diagram of the connections and conventions of an ideal, two-pole, three-phase, symmetrical induction machine and its magnetic axes representations are shown in Figs. III-1 and III-2, respectively.

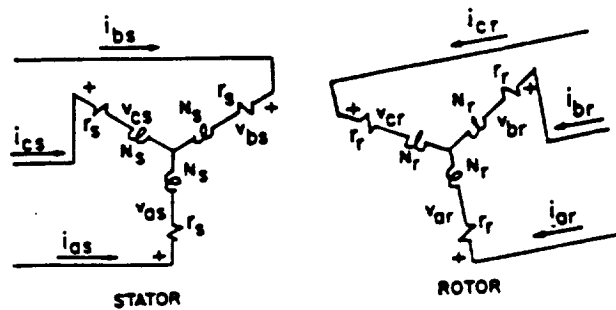


Fig. III-1 - Connections and Current Conventions for Three-Phase Induction Motor

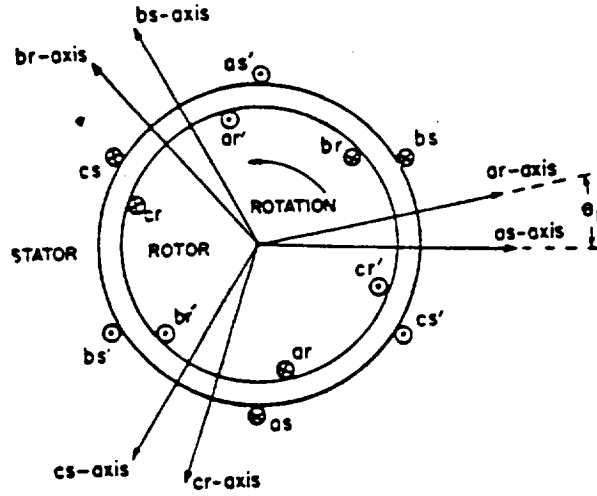


Fig. III-2 - Relative Positions of the Magnetic Axes of Stator and Rotor Windings.

With the appropriate subscript for the stator (as, bs, cs) and rotor (ar, br, cr) phases, the following voltage eqn. (12) is applicable to each of the six windings shown in Fig.III-2.

$$v = p * \lambda + r * i \quad (12)$$

where λ , r and p are the total flux linkage, the winding resistance and the differential operator d/dt , respectively.

The flux-linkage equations[4] for a three-wire machine are summarized in eqn. (13)

$$\begin{bmatrix} \lambda_{as} \\ \lambda_{bs} \\ \lambda_{cs} \\ \lambda_{ar} \\ \lambda_{br} \\ \lambda_{cr} \end{bmatrix} = \begin{bmatrix} L_{ss} & 0 & 0 \\ 0 & L_{ss} & 0 \\ 0 & 0 & L_{ss} \\ L_{sr} \cos \theta_r & L_{sr} \cos \left(\theta_r - \frac{2\pi}{3} \right) & L_{sr} \cos \left(\theta_r + \frac{2\pi}{3} \right) \\ L_{sr} \cos \left(\theta_r + \frac{2\pi}{3} \right) & L_{sr} \cos \theta_r & L_{sr} \cos \left(\theta_r - \frac{2\pi}{3} \right) \\ L_{sr} \cos \left(\theta_r - \frac{2\pi}{3} \right) & L_{sr} \cos \left(\theta_r + \frac{2\pi}{3} \right) & L_{sr} \cos \theta_r \\ L_{rr} \cos \theta_r & L_{rr} \cos \left(\theta_r + \frac{2\pi}{3} \right) & L_{rr} \cos \left(\theta_r - \frac{2\pi}{3} \right) \\ L_{rr} \cos \left(\theta_r - \frac{2\pi}{3} \right) & L_{rr} \cos \theta_r & L_{rr} \cos \left(\theta_r + \frac{2\pi}{3} \right) \\ L_{rr} \cos \left(\theta_r + \frac{2\pi}{3} \right) & L_{rr} \cos \left(\theta_r - \frac{2\pi}{3} \right) & L_{rr} \cos \theta_r \\ L_{rr} & 0 & 0 \\ 0 & L_{rr} & 0 \\ 0 & 0 & L_{rr} \end{bmatrix} \times \begin{bmatrix} i_{as} \\ i_{bs} \\ i_{cs} \\ i_{ar} \\ i_{br} \\ i_{cr} \end{bmatrix} \quad (13)$$

where

$$L_{SS} = L_S - L_{Sm} \quad ; \quad L_{rr} = L_r - L_{rm}$$

The parameters L_{sm} and L_{rm} are the mutual inductances between the individual stator and individual rotor phases, respectively. The term θ_r is the angular displacement between corresponding phases of the stator and rotor axes, as shown in Fig. III-2. The time varying coefficients in eqn. (13) may be eliminated by means of transformation equations.

III.2 Transformation to d-q Variables

Fig. III-3 illustrates the angular relation of the stator and rotor axes relative to an orthogonal set of d-q axes. The transformation axes are rotating at an arbitrary electrical angular velocity, ω . It is noteworthy that the stator as-bs-cs set is fixed in the stator. Similarly, the ar-br-cr set is fixed in the rotor and, thus, rotates at the rotor electrical angular velocity, ω_r .

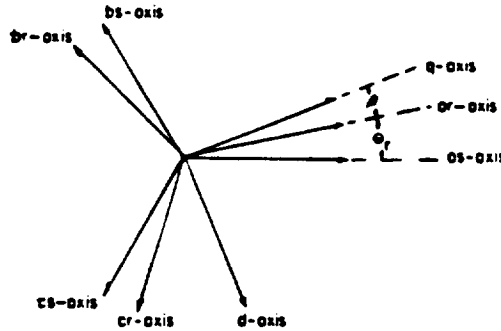


Fig. III-3 - Axis of 2-pole, 3-phase symmetrical machine.

In conjunction with Fig. III-3, and by means of geometric projections, it can be shown that the transformation from the machine a, b, c co-ordinates to the d-q reference frame is given by eqn. (14),

$$\begin{bmatrix} f_{qs} \\ f_{ds} \\ f_{os} \\ f_{qr} \\ f_{dr} \\ f_{or} \end{bmatrix} = \frac{2}{3} \begin{bmatrix} \cos(\theta) & \cos(\theta - 2\pi/3) & \cos(\theta + 2\pi/3) \\ \sin(\theta) & \sin(\theta - 2\pi/3) & \sin(\theta + 2\pi/3) \\ 1/2 & 1/2 & 1/2 \\ \text{---} & \text{---} & \text{---} \\ [0] & \cos(\beta) & \cos(\beta - 2\pi/3) & \cos(\beta + 2\pi/3) \\ \text{---} & \sin(\beta) & \sin(\beta - 2\pi/3) & \sin(\beta + 2\pi/3) \\ \text{---} & 1/2 & 1/2 & 1/2 \end{bmatrix} \begin{bmatrix} f_{as} \\ f_{bs} \\ f_{cs} \\ f_{ar} \\ f_{br} \\ f_{cr} \end{bmatrix} \quad (14)$$

where $\beta = \theta - \theta_r$, (15)

and θ is a continuous function. In these equations, the variable 'f' represents either voltage, current, or flux-linkage.

III.3 Reference Frames

III.3.1 Arbitrary Reference Frames

The transformation equation (14) may be used to transform the stator and rotor voltages and currents of eqns (12) and (13) to the form shown in eqn. (16).

$$\begin{bmatrix} v_{ds} \\ v_{qs} \\ v'_{dr} \\ v'_{qr} \end{bmatrix} = \begin{bmatrix} r_s + L_{ss} * p & -\omega * L_{ss} & M * p & -\omega * M \\ \omega * L_{ss} & r_s + L_{ss} * p & \omega * M & M * p \\ M * p & -(\omega - \omega_r)M & r'_r + L'_{rr} * p & -(\omega - \omega_r)L'_{rr} \\ (\omega - \omega_r)M & M * p & (\omega - \omega_r)L'_{rr} & r'_r + L'_{rr} * p \end{bmatrix} * \begin{bmatrix} i_{ds} \\ i_{qs} \\ i'_{dr} \\ i'_{qr} \end{bmatrix} \quad (16)$$

By setting the speed ω , of the arbitrary reference frame, in eqn. (16), equal to the speed of the desired reference frame, the voltage equations may be expressed in any reference frame. The stationary or stator reference frame voltage equations may be obtained by setting ω equal to zero in eqn. (16). Setting ω equal to ω_r , the electrical angular velocity of the rotor, gives a reference frame fixed in the rotor.

III.3.2 Synchronous Rotating Reference Frame

The synchronously rotating reference frame voltage equations are obtained by setting ω equal to the electrical angular velocity, ω_e , of the fundamental frequency components of the applied stator voltages. This substitution yields equation (17).

$$\begin{bmatrix} v_{ds} \\ v_{qs} \\ v_{dr}^{\prime} \\ v_{qr}^{\prime} \end{bmatrix} = \begin{bmatrix} r_s + L_{ss} * p & -\omega_e * L_{ss} & M * p & -\omega_e * M \\ \omega_e * L_{ss} & r_s + L_{ss} * p & \omega_e * M & M * p \\ M * p & -(\omega_e - \omega_r) M & r_r' + L_{rr}' * p & -(\omega_e - \omega_r) L_{rr}' \\ (\omega_e - \omega_r) M & M * p & (\omega_e - \omega_r) L_{rr}' & r_r' + L_{rr}' * p \end{bmatrix} * \begin{bmatrix} i_{ds} \\ i_{qs} \\ i_{dr}^{\prime} \\ i_{qr}^{\prime} \end{bmatrix} \quad (17)$$

All entries in the impedance matrix of either eqn. (17) or (16) are in actual units. For steady-state operation, the operator 'p' is replaced by the appropriate 'j ω_a ' term where ω_a is the frequency of the voltages in the transformed frame.

III.3.3 Multiple Reference Frame

The voltage equations are linear if constant rotor speed is assumed. In that case, the principle of superposition can be used to obtain the machine performance due to the total harmonic content in the source voltages. For balanced sinusoidal applied voltages, the synchronously rotating d-q transformed voltages become constant voltages. This can be verified via application of eqn. (14) to such input source voltages, with the arbitrary speed ω set to the fundamental source frequency ω_e . The resulting constant voltages facilitate computation of constant-speed electrical transients and steady state performance by means of d.c. circuit theory.

In the case of possible harmonic content in the source voltages, each of the harmonic components forms a balanced set of voltages in the synchronously rotating reference frame. Each of these balanced set of voltages becomes constant when transformed to a particular reference frame in which d.c. circuit theory can be used. If this is done, the resulting currents can then be back-transformed to the synchronously rotating reference frame. Subsequently, the final currents can be used to generate the constant-speed performance of the connected machine. Thus, the so-called multiple reference frame [4] application expedites the calculation of steady-state performance from any periodic stator voltage waveforms. Also, it eliminates the need to use phasors and complex impedances.

The synchronously-rotated harmonic voltages, to be derived later, will show that each of the positively rotating voltages (that is fundamental, seventh harmonic, etc.) transforms to a voltage of frequency $(k-1)\omega_e$, where k is the harmonic order. Thus, unity value of k denotes a d.c. or constant value for the transformed fundamental frequency component. Similarly, all negatively rotating voltages (k=5, 11, etc.) transform to voltages with frequency $(k+1)\omega_e$. Hence, the voltage equations for the symmetrical induction machine in any reference frame is given by eqn. (16) in which the arbitrary reference frame speed, ω , is set equal to the speed of the desired frame. When this is done, the resulting multiple reference frame equations are those summarized in eqn. (18). It is emphasized that in eqn. (18), the letter 'n' takes on the value +k or -k, depending on the application of a positive or negative-sequence voltage, respectively. Since d.c. theory applies to all harmonic terms in the respective multiple reference frames, the time-derivative operator 'p' is set to zero in the steady-state performance calculation.

$$\begin{bmatrix} v_{ds} \\ v_{qs} \\ v'_{dr} \\ v'_{qr} \end{bmatrix} = \begin{bmatrix} r_s + L_{SS} * p & -n * \omega_e * L_{SS} & M * p & -n * \omega_e * n * M \\ n * \omega_e * n * L_{SS} & r_s + L_{SS} * p & n * \omega_e * n * M & M * p \\ M * p & -(n * \omega_e - \omega_r) M & r'_r + L'_{rr} * p & -(n * \omega_e - \omega_r) L'_{rr} \\ (n * \omega_e - \omega_r) M & M * p & (n * \omega_e - \omega_r) L'_{rr} & r'_r + L'_{rr} * p \end{bmatrix} * \begin{bmatrix} i_{ds} \\ i_{qs} \\ i'_{dr} \\ i'_{qr} \end{bmatrix} \quad (18)$$

[V] [Z] [I]

The impedance matrix, [Z], of eqn. (18) has been used for computer simulation to verify some published results. For ease of comparison, the [Z] matrix has been per-unitized and expressed in eqn. (19).

$$[Z] = \begin{bmatrix} r_s & -fr * n * X_{SS} & 0 & -fr * n * X_m \\ fr * n * X_{SS} & r_s & fr * n * X_m & 0 \\ 0 & -akf * fr * X_m & r'_r & -akf * fr * X'_{rr} \\ akf * fr * X_m & 0 & akf * fr * X'_{rr} & r'_r \end{bmatrix} \quad (19)$$

where the per-unit values in eqn. (19) are defined below, namely

$$fr = \omega_e / \omega_b$$

$$fr * X_{SS} = (\omega_e / \omega_b) * \omega_b * L_{SS}$$

$$fr * X_m = (\omega_e / \omega_b) * \omega_b * M$$

$$fr * X'_{rr} = (\omega_e / \omega_b) * \omega_b * L'_{rr}$$

$$akf = n - (\omega_r / \omega_e)$$

$$(n \omega_e - \omega_r) M = (n - \omega_r / \omega_e) fr * X_m = akf * fr * X_m$$

$$M p = j(k-+1) * (\omega_e / \omega_b) * \omega_b * M = j(k-+1) fr * X_m$$

III.4 Derivation of Multiple Reference Frame Voltages

Consider a three-phase machine operated from a balanced source with a fundamental frequency, ω_e . Using eqn. (13), the d-q stator voltages fixed in the stator ($\theta = 0$) are given by eqn (20).

$$\begin{bmatrix} v^s_{ds} \\ v^s_{qs} \end{bmatrix} = \frac{2}{3} \begin{bmatrix} 0 & \sqrt{3}/2 & -\sqrt{3}/2 \\ 1 & -1/2 & 1/2 \end{bmatrix} * \begin{bmatrix} v_{as} \\ v_{bs} \\ v_{cs} \end{bmatrix} \quad (20)$$

i.e.

$$v^s_{ds} = 1/\sqrt{3}(v_{bs} - v_{cs})$$

$$v^s_{qs} = v_{as}$$

For a harmonic-rich source, the input voltages are periodic and sinusoidal. Hence, eqn. (21) gives the Fourier expansion of the transformed voltages.

$$\begin{aligned} v^s_{ds} &= \sum_{k=1}^{\infty} \{ v_{kdc} \cos(k\omega_e t) + v_{kds} \sin(k\omega_e t) \} \\ v^s_{qs} &= \sum_{k=1}^{\infty} \{ v_{kqc} \cos(k\omega_e t) + v_{kqs} \sin(k\omega_e t) \} \end{aligned} \quad (21)$$

When expressed in terms of the voltages v^s_{ds} and v^s_{qs} , the applied stator voltages in the synchronously rotating frame are shown in eqn. (22).

$$\begin{aligned} v^e_{ds} &= v^s_{qs} \sin(\omega_e t) + v^s_{ds} \cos(\omega_e t) = v^{+e}_{kds} + v^{-e}_{kds} \\ v^e_{qs} &= v^s_{qs} \cos(\omega_e t) - v^s_{ds} \sin(\omega_e t) = v^{+e}_{kqs} + v^{-e}_{kqs} \end{aligned} \quad (22)$$

Substitution of eqn. (21) into eqn. (22) will show that the voltages v^{+e}_{kds} and v^{+e}_{kqs} of the positive sequence applied voltages form a series of balanced sets. For $k > 1$, these sets rotate at an electrical angular velocity of $(k-1)\omega_e$ in the counterclockwise direction with regard to the synchronously rotating frame. Similarly, v^{-e}_{kds} and v^{-e}_{kqs} of the negative sequence applied voltages rotate at the frequency $-(k+1)\omega_e$ in the clockwise direction with respect to the synchronously rotating reference frame.

In a manner consistent with the forms in eqn. (22), the “+ke” variables in the multiple reference frame are obtained from the “+e” of the synchronously rotating reference by use of eqns. (23) and (24). [4],

$$\begin{bmatrix} f_{ds}^{+ke} \\ f_{qs}^{+ke} \\ f_{dr}^{+ke} \\ f_{qr}^{+ke} \end{bmatrix} = \begin{bmatrix} \cos\{(k-1)\omega_e^* t\} & \sin\{(k-1)\omega_e^* t\} & & \\ -\sin\{(k-1)\omega_e^* t\} & \cos\{(k-1)\omega_e^* t\} & & \\ & & [0] & \\ & & & \cos\{(k-1)\omega_e^* t\} \sin\{(k-1)\omega_e^* t\} \\ & & & -\sin\{(k-1)\omega_e^* t\} \cos\{(k-1)\omega_e^* t\} \\ & [0] & & \end{bmatrix} * \begin{bmatrix} f_{kds}^{+e} \\ f_{kqs}^{+e} \\ f_{kdr}^{+e} \\ f_{kqr}^{+e} \end{bmatrix} \quad (23)$$

$$\begin{bmatrix} f_{ds}^{-ke} \\ f_{qs}^{-ke} \\ f'_{dr}{}^{-ke} \\ f'_{qr}{}^{-ke} \end{bmatrix} = \begin{bmatrix} \cos((k+1)\omega_e^*t) & -\sin((k+1)\omega_e^*t) & & \\ \sin((k+1)\omega_e^*t) & \cos((k+1)\omega_e^*t) & & [0] \\ \text{-----} & \text{-----} & \text{-----} & \text{-----} \\ & & \cos((k+1)\omega_e^*t) & -\sin((k+1)\omega_e^*t) \\ & [0] & \sin((k+1)\omega_e^*t) & \cos((k+1)\omega_e^*t) \end{bmatrix} * \begin{bmatrix} f_{kds}^{-e} \\ f_{kqs}^{-e} \\ f'_{kdr}{}^{-e} \\ f'_{kqr}{}^{-e} \end{bmatrix} \quad (24)$$

where $f_{ds}^{+ke}, f_{qs}^{+ke}$ represent variables in the multiple reference frame, and $f_{kds}^{+e}, f_{kqs}^{+e}$ represent variables in the synchronous reference frame. It is noteworthy that, for stator only-fed induction machine, the rotor windings are shorted. Hence, for voltage representation, v_{ar}, v_{br} , and v_{cr} are 0. Consequently, so are all the rotor variables subscripted "dr", etc. in eqns. (23) and (24).

Eqns. (25) represent a given set of 3 phase, balanced nonsinusoidal voltages,

$$v_{as} = \Sigma\{V_k * \cos(k * \omega_e^*t)\},$$

$$v_{bs} = \Sigma\{V_k * \cos[k(\omega_e^*t - 2\pi/3)]\}, \quad (25)$$

$$v_{cs} = \Sigma\{V_k * \cos[k(\omega_e^*t + 2\pi/3)]\},$$

where $k = 1, 5, 7, 11, \dots$

The synchronously rotating reference frame voltages are as expressed in eqn. (26),

$$\begin{bmatrix} v_{kds}^{e+-} \\ v_{kqs}^{e+-} \\ v'_{kdr}{}^{e+-} \\ v'_{kqr}{}^{e+-} \end{bmatrix} = \begin{bmatrix} -+V_{k+-} * \sin((k -+ 1)\omega_e t) \\ V_{k+-} * \cos((k -+ 1)\omega_e t) \\ 0 \\ 0 \end{bmatrix} \quad (26)$$

where the positive superscripts refer to positive-sequence applied voltages, $k_+ = 1, 7, 13, \dots$ and the negative superscripts denote negative-sequence applied voltages, $k_- = 5, 11, \dots$. The variable V_{k+-} represents the magnitude of the appropriate source harmonic voltage applied to the machine. Comparison of eqns. (23) and (24) and (26) shows that, for voltage considerations, eqn. (27) holds.

$$[f^{+e}_{kds} \quad f^{+e}_{kqs} \quad f^{+e}_{kdr} \quad f^{+e}_{kqr}]^T \equiv [v^{e}_{dsk+} \quad v^{e}_{qsk+} \quad v'^{e}_{drk+} \quad v'^{e}_{qrk+}]^T \quad (27)$$

$$[f^e_{kds} \quad f^e_{kqs} \quad f^e_{kdr} \quad f^e_{kqr}]^T \equiv [v^e_{dsk-} \quad v^e_{qsk-} \quad v'^e_{drk-} \quad v'^e_{qrk-}]^T$$

Thus, substitution of eqn. (26) into eqns. (23) and (24) gives the multiple reference frame voltages in eqn. (28).

$$\begin{bmatrix} v_{ds}^{+-ke} \\ v_{qs}^{+-ke} \\ v'_{dr}{}^{+-ke} \\ v'_{qr}{}^{+-ke} \end{bmatrix} = \begin{bmatrix} 0 \\ V_{k+-} \\ 0 \\ 0 \end{bmatrix} \quad (28)$$

The impedance matrix of eqn. (17) and the voltage magnitudes of eqn. (26) may be used to simulate the machine performance in the synchronously rotating reference frame.

For steady state operation, the operator 'p' in the impedance matrix is replaced by "j(k₊-1)ω_e" for stator applied positive sequence voltages, and "j(k₊+1)ω_e" for negative sequence voltages. For simulation in the multiple reference frame, eqns. (19) and (28) are used. It may be recalled from section III.3.3 that all p-dependent terms are non-existent due to the resulting time-invariant voltages in the multiple reference frame. The following section discusses some simulation results.

IV. SIMULATION RESULTS

Results of computer simulations of a symmetrical induction machine are described for the various drive sources discussed in section II. The developed computer algorithm for the simulation is flow-charted in Appendix A1.

IV.1 Parameters of Induction Machine

The following values in Table I are used for simulating the impedance matrix in the multiple reference frame. All values are in per-unit[4] unless otherwise stated.

TABLE I - Summary of Induction Machine Parameters

| Parameter | Value [‡] |
|-------------------------------|-------------------------|
| r_s | 0.0453 |
| r'_r | 0.0222 |
| X_{ls} | 0.0775 |
| X'_{lr} | 0.0322 |
| X_m | 2.0420 |
| $X_{ss} = X_{ls} + X_m$ | 2.1195 |
| $X'_{rr} = X'_{lr} + X_m$ | 2.0742 |
| ω_b | $2\pi*60$ rad/s |
| $f_r = \omega_e / \omega_b$ | 1.0 |
| s | 0.03 |
| $\omega_r = \omega_e*(1 - s)$ | $(2\pi*60)(0.97)$ rad/s |

s - slip ; ω_b - base electrical angular velocity

[‡] per-unit values unless stated otherwise

IV.2. Six-Step Induction Motor Drive

The simulation of a six-step induction motor drive seeks to validate the derived analytic relations and computer algorithm by comparing the simulated results with published data. The source input voltages are taken from reference[4]. The harmonic voltage magnitudes in the multiple reference frame are indicated in Table II. Note that the rotor voltages are zero due to shorting of the rotor windings. Also, consistent with eqn. (28), only the q-axis voltages exist in the multiple reference frame.

TABLE II -Six-Step Voltage Magnitudes in Multiple Reference Frame

| <u>Harmonic Order</u> | <u>Value(pu)</u> |
|-----------------------|------------------|
| v^{+1e}_{qs} | $4 / \pi$ |
| v^{-5e}_{qs} | $4 / 5 \pi$ |
| v^{+7e}_{qs} | $- 4 / 7 \pi$ |
| v^{-11e}_{qs} | $- 4 / 11 \pi$ |
| v^{+13e}_{qs} | $4 / 13 \pi$ |

The inverter constant input voltage V , set to 1.0 pu for the simulation, is the amplitude of the

balanced squarewave voltages at the source.

Table III shows a comparison between the published[4] and calculated steady-state currents in the multiple reference frame. The current values are corrected to the third decimal place. With the exception of the fundamental frequency components, the remaining calculated currents correlate reasonably with the published results. The discrepancy in the fundamental frequency currents is discussed later in conjunction with line current and electrical torque plots.

TABLE III - Comparison of Calculated and Published Per-Unit d-q Currents

| <i>n</i> (+/-k) | <i>i^{ne}_{ds}</i> | | <i>i^{ne}_{qs}</i> | | <i>i^{ne}_{dr}</i> | | <i>i^{ne}_{qr}</i> | |
|--------------------|------------------------------------|---------|------------------------------------|---------|------------------------------------|---------|------------------------------------|---------|
| | Ref[4] | Calc. | Ref[4] | Calc. | Ref[4] | Calc. | Ref[4] | Calc. |
| +1 | 0.600 | 0.74120 | 0.013 | 1.50260 | 0 | -0.1791 | 0 | -1.5432 |
| -5 | -0.460 | -0.4602 | 0.053 | 0.053 | 0.453 | 0.453 | -0.053 | -0.0533 |
| +7 | -0.2360 | -0.2360 | -0.022 | -0.022 | 0.232 | 0.232 | 0.022 | 0.022 |
| -11 | 0.096 | 0.096 | -0.005 | -0.005 | -0.095 | -0.095 | 0.005 | 0.005 |
| +13 | 0.069 | 0.069 | 0.003 | 0.003 | -0.068 | -0.068 | -0.003 | -0.003 |

Using the steady state currents shown in Table III, one can calculate the instantaneous stator and rotor phase currents and torque from eqns. (29) to (33).

$$i_{as} = i_{qs} = \Sigma[(i_{qs}^{+ke} + i_{qs}^{-ke})\cos(k*\omega_e*t) + (i_{ds}^{+ke} - i_{ds}^{-ke})\sin(k*\omega_e*t)] \quad (29)$$

$$i_{ds} = \Sigma[(i_{ds}^{+ke} + i_{ds}^{-ke})\cos(k*\omega_e*t) - (i_{qs}^{+ke} - i_{qs}^{-ke})\sin(k*\omega_e*t)] \quad (30)$$

$$i'_{qr} = \Sigma[(i'_{qr}{}^{+ke} + i'_{qr}{}^{-ke})\cos(k*\omega_e*t) + (i'_{dr}{}^{+ke} - i'_{dr}{}^{-ke})\sin(k*\omega_e*t)] \quad (31)$$

$$i'_{dr} = \Sigma[(i'_{dr}{}^{+ke} + i'_{dr}{}^{-ke})\cos(k*\omega_e*t) - (i'_{qr}{}^{+ke} - i'_{qr}{}^{-ke})\sin(k*\omega_e*t)] \quad (32)$$

$$T = M * (m/2) * (P/2) * [i_{qs} * i'_{dr} - i_{ds} * i'_{qr}], \quad (33)$$

where

P = number of poles = 2
m = number of phases = 3,
M = *X_m* from impedance matrix

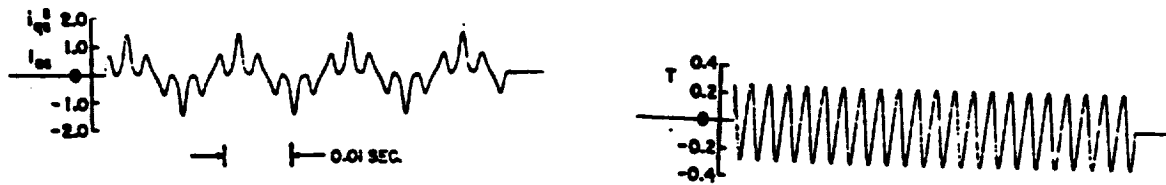
Substitution of eqns. (29) through (32) into (33) yields a torque expression which contains a constant term and second harmonic components of the source constituent harmonics superimposed on it. The expanded torque expression appears in eqn. (34).

$$\begin{aligned}
T = M (m/2) (P/2) S \{ & (i^{+ke}_{qs} * i'^{+ke}_{dr} + i^{-ke}_{qs} * i'^{-ke}_{dr}) - (i^{+ke}_{ds} * i'^{+ke}_{qr} + i^{-ke}_{ds} * i'^{-ke}_{qr}) \\
& + [(i^{+ke}_{qs} * i'^{-ke}_{dr} + i^{-ke}_{qs} * i'^{+ke}_{dr}) - (i^{+ke}_{ds} * i'^{-ke}_{qr} + i^{-ke}_{ds} * i'^{+ke}_{qr})] \cos(2k\omega_e t) \\
& + [(i^{+ke}_{qs} * i'^{-ke}_{qr} + i^{+ke}_{ds} * i'^{-ke}_{dr}) - (i^{-ke}_{ds} * i'^{+ke}_{dr} + i^{-ke}_{qs} * i'^{+ke}_{qr})] \sin(2k\omega_e t) \quad (34)
\end{aligned}$$

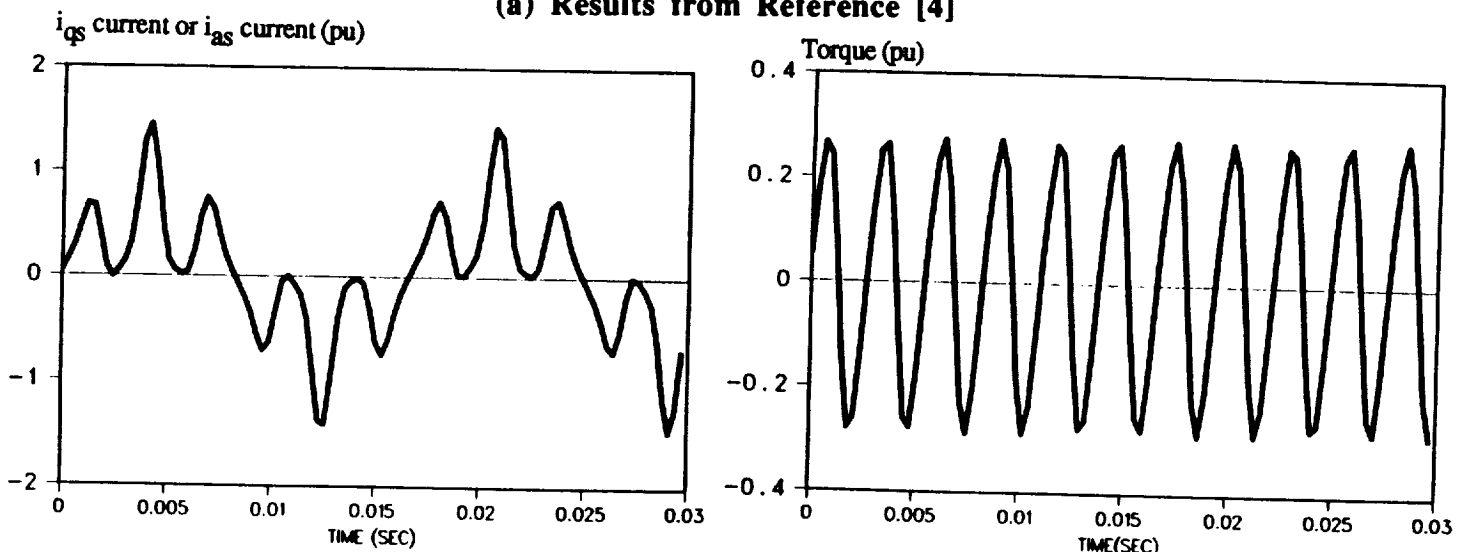
Computer simulation results of the instantaneous phase A current and electrical torque are depicted in Figs. IV-1 and IV-2. The plots in Fig. IV-1 pertain to a comparison between the simulated (b) and published (a) results. The simulated plots are obtained from values in Table III and the expressions in eqns. (29) and (33). The plots shown in Fig. IV-1(a) are taken directly from reference[4]. As pointed out earlier, the calculated d-q harmonic current components match the published data in Table III. The d-q fundamental current components used in the simulation of Fig IV-1(a) are those from reference [4]. Satisfactory correlaton is evident between the simulated and published plots. The torque pulsation is due to the harmonic content of the distorted current. The slight discrepancy in the peak values is attributed to truncation in the number of harmonic source voltages included in the simulation. Of particular interest is the absence of a dc offset in the torque plots. This is inconsistent with the torque eqn. (34).

A repeat of the simulated results is illustrated in Fig. IV-2(b). Here, the simulated d-q fundamental current components, rather than the published values, are used in eqn. (29). These results are compared with those from reference[6], depicted in Fig. IV-2(a). The source voltage magnitudes from reference[6] are neither the same as those from reference [5] or those used in the simulation.

It is evident that the basic form of the results from the simulation and reference[6] are very similar. Furthermore, the torque plots from the simulation and reference[6] clearly demonstrate the d.c offset embodied in the torque expression of eqn. [34]. This suggests a possible error in the reported d-q fundamental current components in reference[5].

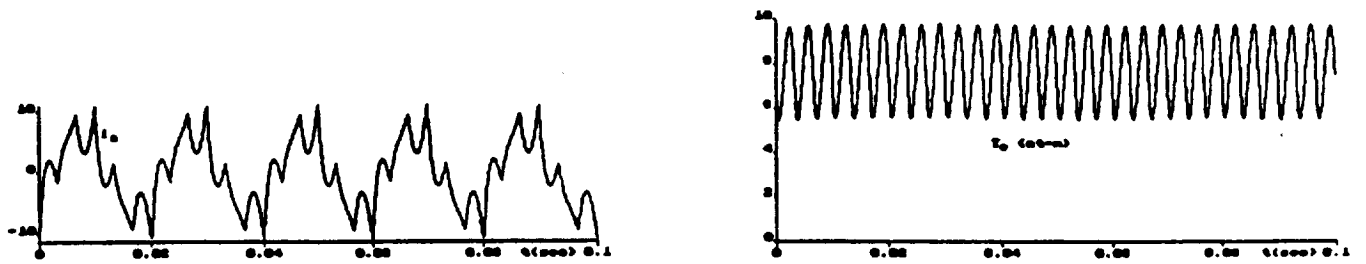


(a) Results from Reference [4]

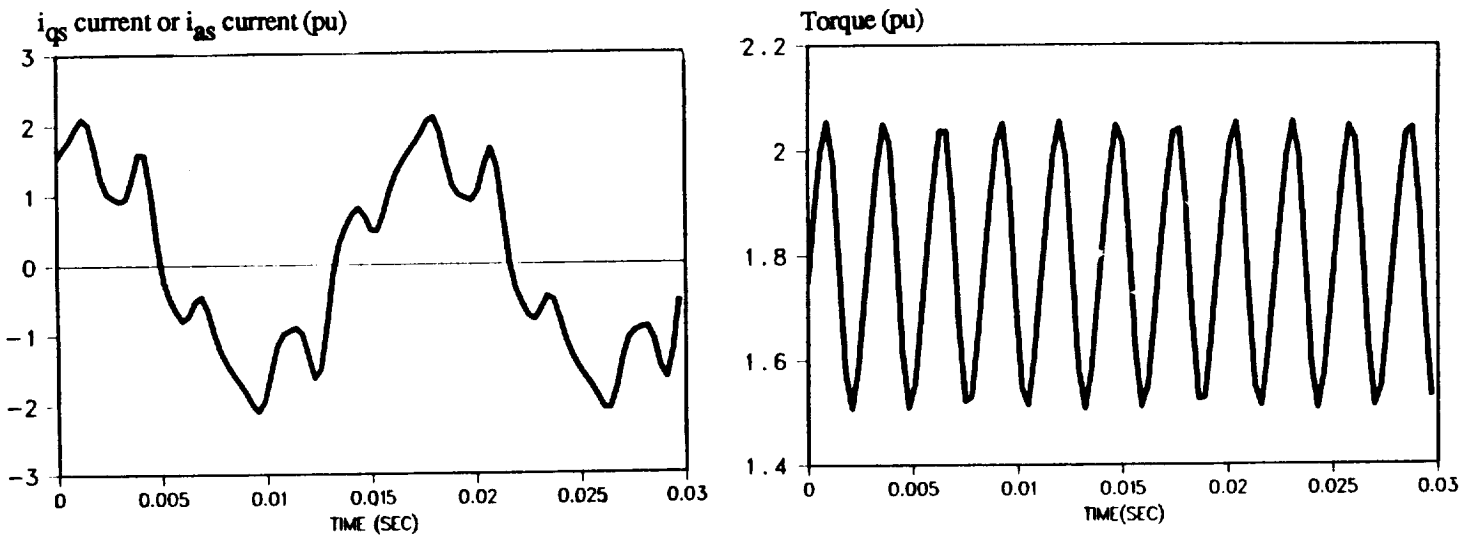


(b) Results from Simulation

FIG. IV-1 - Synchronous Speed Operation Using Multiple Reference Frame Approach and Six-Step Inverter Induction Motor Drive



(a) Results from Reference [6]



(b) Results from Simulation

FIG. IV-2 - Results of Six-Step Inverter Induction Motor Drive Simulation

IV.3. PWMI - Induction Machine Drive

The simulated per-unit harmonic voltages, using the analytic relations outlined in Section II.1 are summarized in Table IV for two operating frequencies, 12 and 54 Hz. The resulting multiple reference frame currents for the 12Hz operation are shown in Table V.

| Harmonic Order, k | Freq. W (Hz) | 12 | 54 |
|-------------------|--------------|----------|-----------------------|
| | | Per-Unit | Line-Neutral Voltages |
| 1 | | 0.221 | 1.002 |
| 5 | | 0.046 | 0.272 |
| 7 | | 0.034 | 0.085 |
| 11 | | 0.024 | 0.091 |
| 13 | | 0.022 | 0.121 |

TABLE IV - Computer Results of Synthesized Pulse Width Modulation Inverter

| $n(+k)$ | i^{ne}_{ds} | i^{ne}_{qs} | i^{ne}_{dr} | i^{ne}_{qr} |
|---------|---------------|---------------|---------------|---------------|
| +1 | 0.12860 | 0.2606 | -0.0311 | -0.2676 |
| -5 | -0.0825 | 0.0096 | 0.08120 | -0.0096 |
| +7 | 0.04380 | 0.0040 | -0.0431 | -0.0040 |
| -11 | -0.0200 | 0.0011 | 0.01970 | -0.0011 |
| +13 | 0.01570 | 0.0008 | -0.0154 | -0.0008 |

TABLE V - PWMI Steady-State Per-Unit Currents in Multiple Reference Frame (12Hz Operation)

Substituting the steady state currents from Table V into eqns. (29) - (33) gives the simulated instantaneous currents, and torque in Fig. IV-4 for the 12Hz operation. The corresponding plots for the 54Hz operation are shown in Fig. IV-5.

Fig. IV-4 shows the instantaneous current and torque for the 12Hz case, while fig. IV-5 shows the same graphs for the 54Hz case.

Both Figs. IV-4 and IV-5 display similar harmonic distortion in the current waveforms, and pulsations in the torque. However, no direct comparison can be made with the six-step drive results, since no direct correspondence exists in the resulting voltages of the two drives simulated. Hence, no attempt has been made to put the plots on the same scale for comparison.

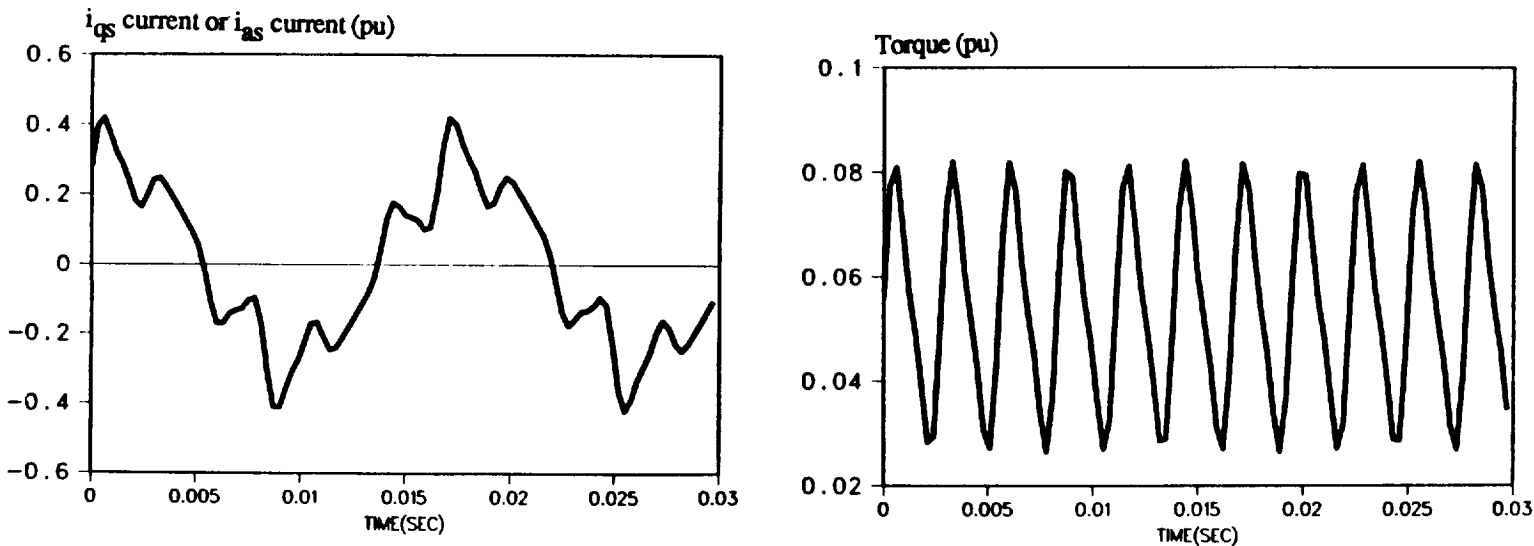


FIG. IV-4 - Steady-State Operation Using PWMI : 12Hz

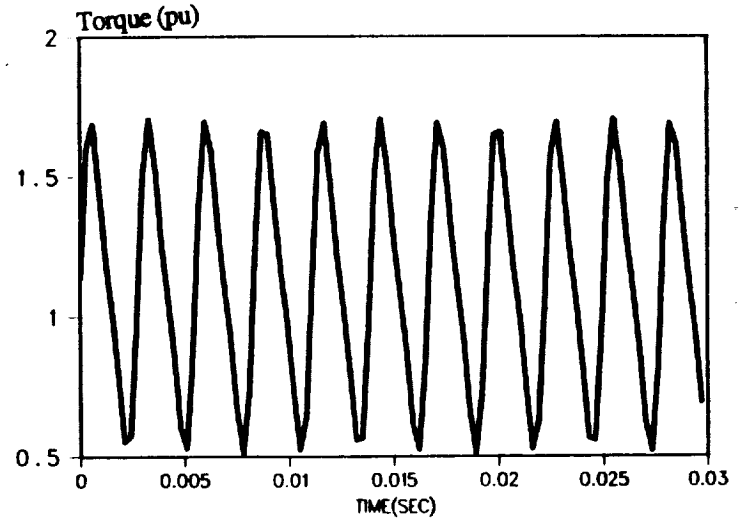
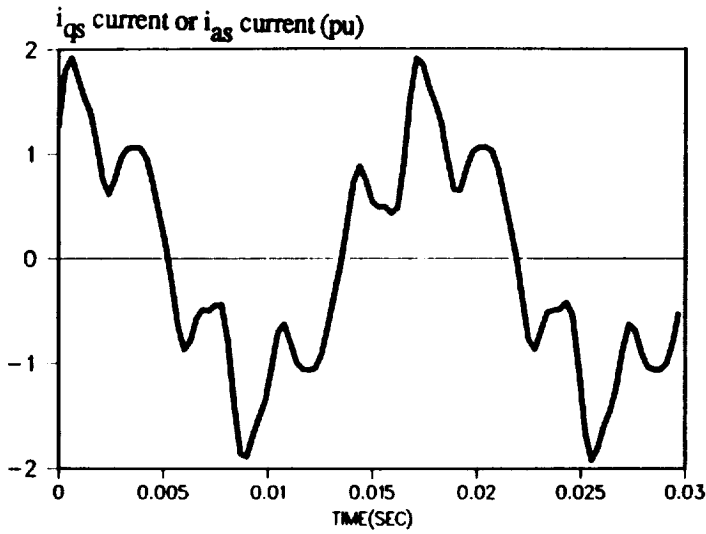


FIG. IV-5 - Steady-State Operation Using PWMI : 54Hz

IV.4 PDMI - Induction Machine Drive

Table VI shows the results of computer simulations of the analytical voltage expressions derived in section II.3. The steady-state currents in the multiple reference frame are shown in Table VII. These results relate to a high input frequency which is approximately ten times the low output frequency. For this isolated PDMI operation, Table VI shows relatively high harmonic voltage content in the output of the inverter. This high harmonic content is reflected in the current and torque waveform in Fig. IV-6. This observation contradicts the normally-held view of relatively low harmonic content of PDM inverters. However, it must be noted that this brief analysis has not rigorously developed analytic relations for the PDMI in a manner similar to that of the PWMI. Also, the analysis has not been extended to higher output frequencies of the PDMI, which are more than multiples of ten of the input low frequency.

TABLE VI - Computer Results of Pulse Density Modulated Inverter [Derived from waveform in reference[5]]

$$[\omega_{Hf} \approx 10 \omega_{Lf}]$$

| <u>Harmonic Order</u> | <u>Per-Unit Voltage</u> |
|-----------------------|-------------------------|
| 1 | 0.585 |
| 5 | 0.153 |
| 7 | 0.067 |
| 11 | 0.205 |
| 13 | 0.238 |

TABLE VII - PDMI Steady-State Per-Unit Currents in Multiple Reference Frame
 $[\omega_{Hf} \approx 10 \omega_{Lf}]$

| $n(+k)$ | i^{ne}_{ds} | i^{ne}_{qs} | i^{ne}_{dr} | i^{ne}_{qr} |
|---------|---------------|---------------|---------------|---------------|
| +1 | 0.34060 | 0.6905 | -0.0823 | -0.7091 |
| -5 | -0.2760 | 0.0320 | 0.27170 | -0.0320 |
| +7 | 0.08670 | 0.0080 | -0.0854 | -0.0080 |
| -11 | -0.1705 | 0.0092 | 0.16790 | -0.0092 |
| +13 | 0.16690 | 0.0081 | -0.1643 | -0.0081 |

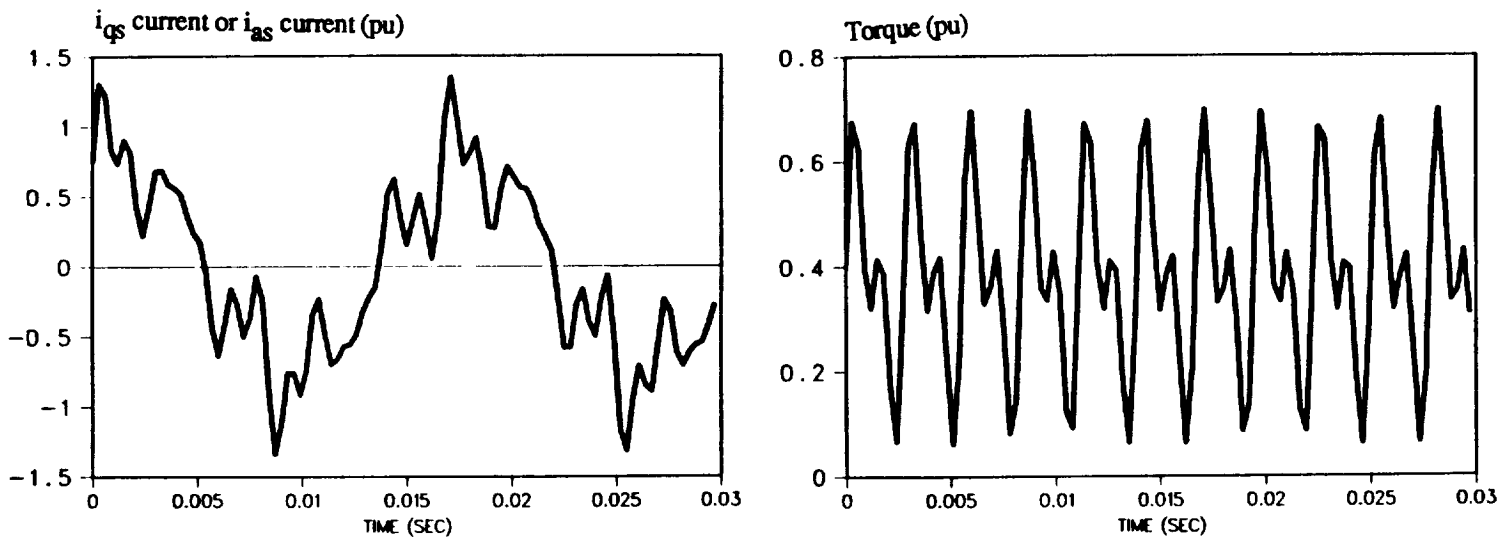


FIG. IV-6 - PDM Results

V.

SUMMARY

This report is a documentation of a computer algorithm developed to analyze variable-frequency A.C. drives. In particular, it contains a synthesis of a pulsewidth modulated inverter(PWMI), and brief descriptions of a six-step inverter and a pulse density modulated inverter(PDMI) drives.

The PWMI source is generated in the algorithm. However, the six-step and PDM inverter sources are simulated by stating their harmonic voltage components obtained from Fourier analysis. A symmetrical induction machine is modeled in the arbitrary, synchronous and multiple reference frames. These models give the flexibility of selecting the most appropriate model for the intended performance prediction.

The algorithm has been verified by a satisfactory correlation between its simulated results and selected data from publications. The harmonic content of the drive sources manifests itself in the form of distorted line currents and pulsating torque. The level of harmonic distortion is determined by the relative magnitudes of the source harmonic voltage magnitudes.

In its present form, the key area of application of the algorithm is the steady-state performance prediction of induction machine-drives. Planned future extensions of the algorithm include the following:

- synthesis and development of analytic expressions for the PDMI and analysis of the effects of various operating frequencies on the A.C. drive performance.

- automatic transformation of source voltages into any of the standard reference frames, for subsequent hook-up to desired A.C. machine model.

- inclusion of other performance parameters, such as operating speed profiles, and total harmonic distortion(THD) of machine currents.

- inclusion of other A.C. machinery models, for possible trade-off studies towards space power applications.

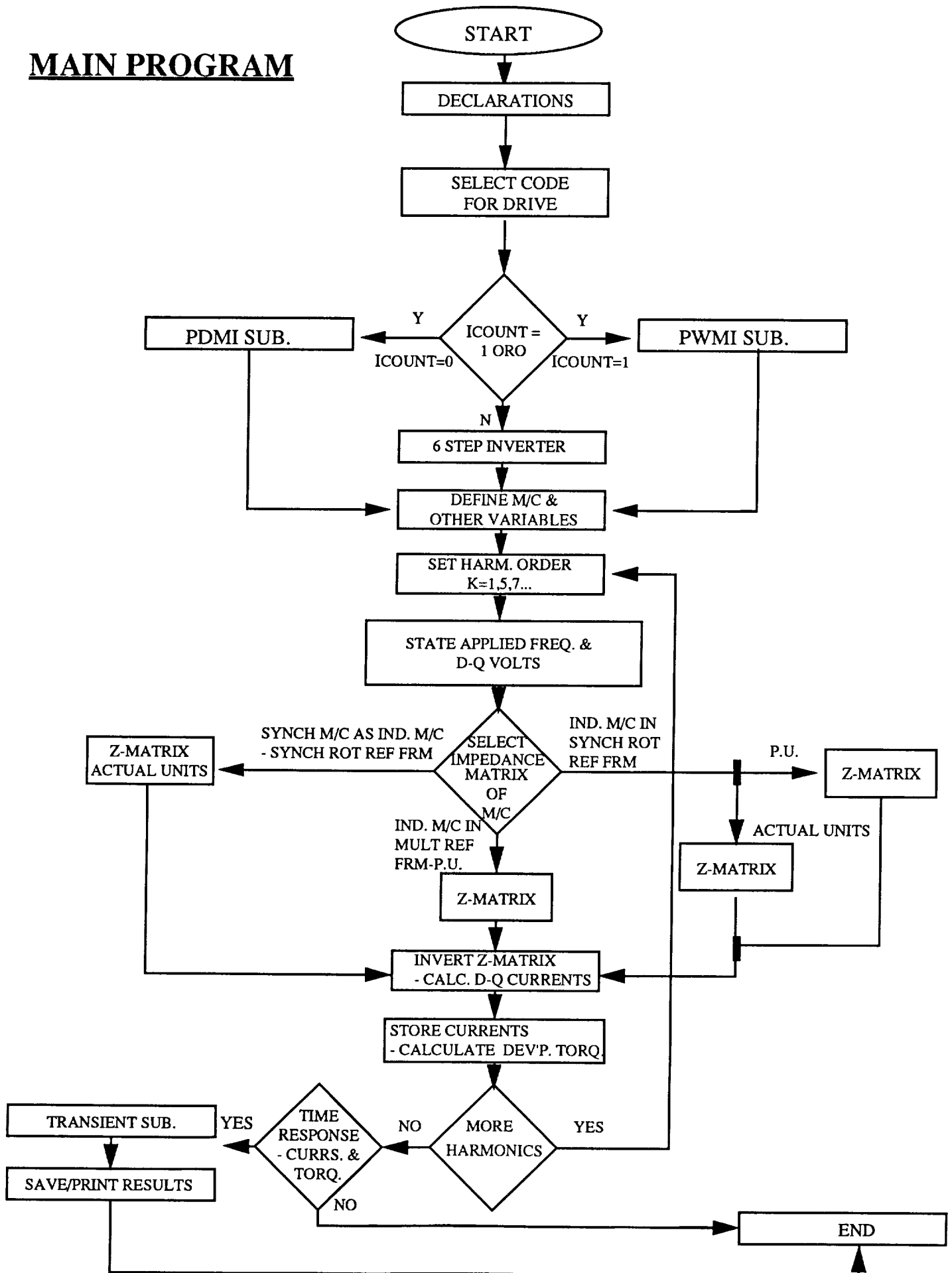
REFERENCES

- [1.] Kankam, M. D. and Tyus, I., "An Efficient Method For Predicting Harmonic Output of Frequency Converters", Report, NASA Lewis Research Center, Summer 1990.
- [2.] Dewan, S.B., Forsythe, J.B., "Harmonic Analysis of a Synchronized Pulse-Width Modulated Three-Phase Inverter", IEEE-IGA Conference Record, Oct. 1971, pp 327-32.
- [3.] Krause, Paul C., Hake, James R., "Method of Multiple Reference Frames Applied to the Analysis of a Rectifier-Inverter Induction Motor Drive", IEEE Trans. on Power Apparatus and Systems, Vol. PAS-88, No. 11, Nov. 1969, pp. 1635-1641.
- [4.] Krause, Paul C., "Method of Multiple Reference Frames Applied to the Analysis of Symmetrical Induction Machinery", IEEE Trans. on Power Apparatus and Systems, Vol. PAS-87, No. 1, Jan. 1968, pp. 218-227.
- [5.] Sood, P.K., Lipo, T.A., Hansen, I.G., "A Versatile Power Converter For High-Frequency Link Systems", IEEE Trans. on Power Electronics, Vol. 3, No. 4, Oct. 1988, pp. 383-390.
- [6.] Lai, Jih-Sheng, "Simnon Simulation for Induciton Motor Drives", 1990 IEEE Paper, TH0301.

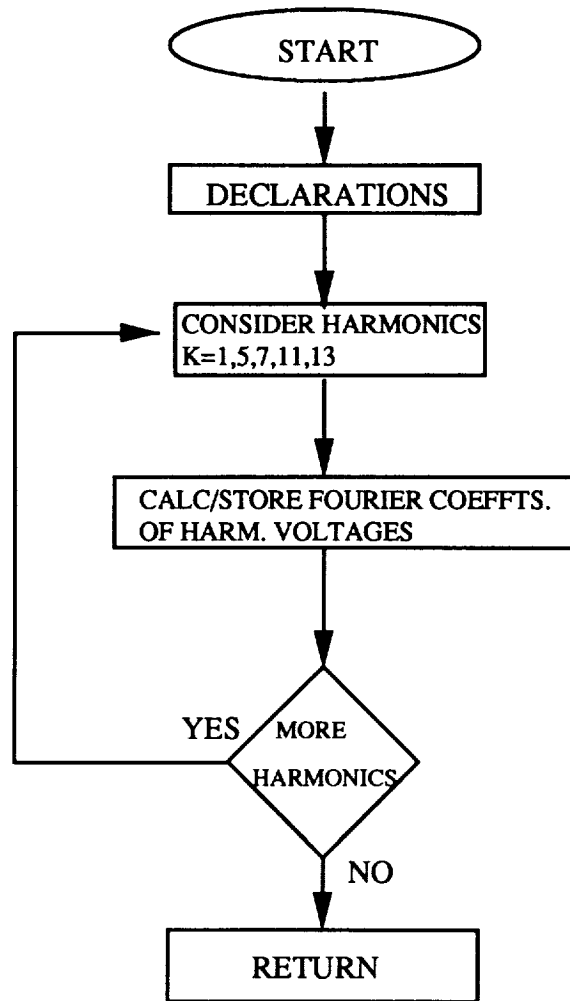
APPENDIX A1

**FLOW CHART
OF
VARIABLE-FREQUENCY A.C. DRIVE**

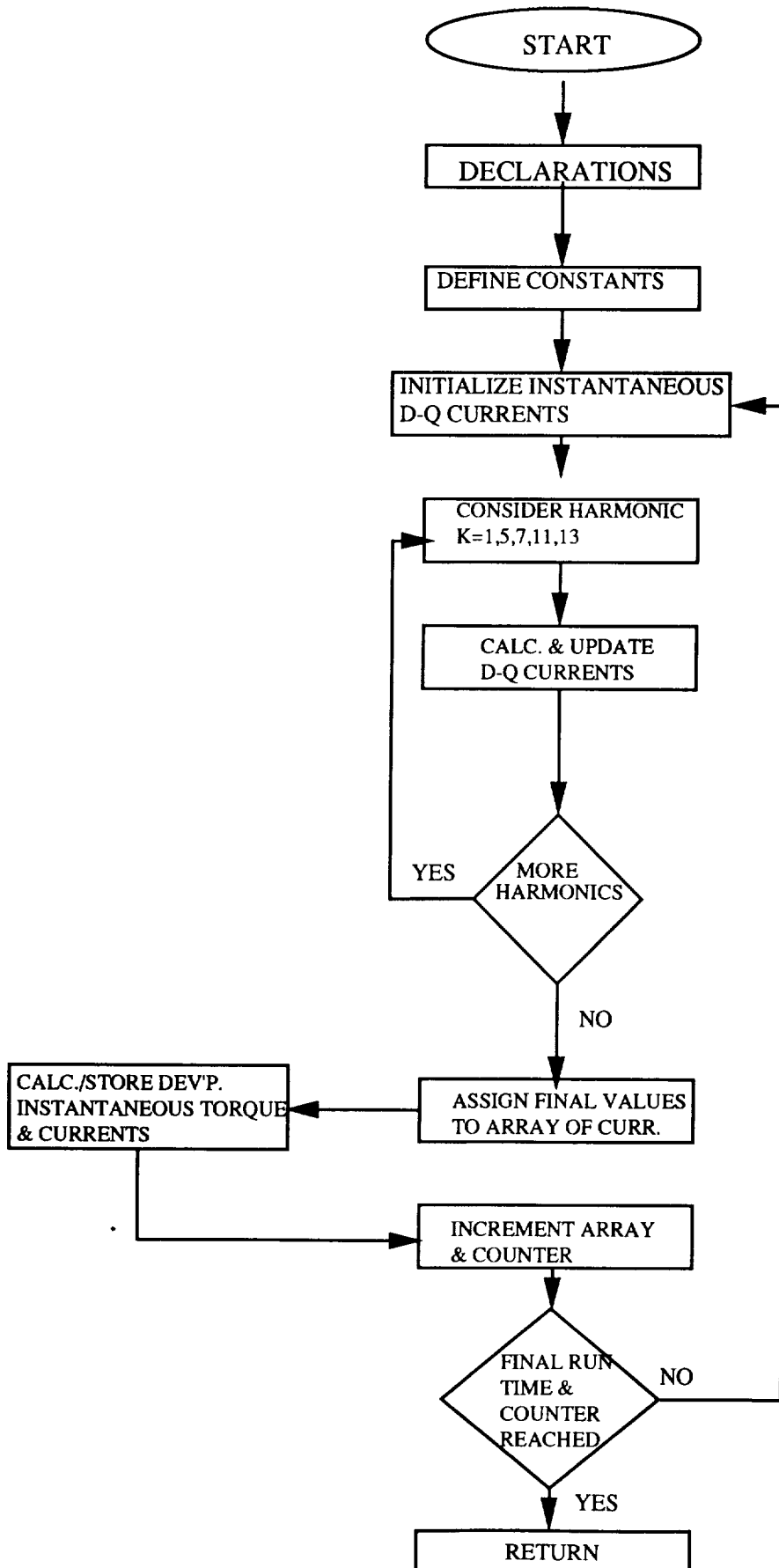
MAIN PROGRAM



PWMI & PDMI
SUBROUTINES



TRANSIENT SUBROUTINE



REPORT DOCUMENTATION PAGE

Form Approved
OMB No. 0704-0188

Public reporting burden for this collection of information is estimated to average 1 hour per response, including the time for reviewing instructions, searching existing data sources, gathering and maintaining the data needed, and completing and reviewing the collection of information. Send comments regarding this burden estimate or any other aspect of this collection of information, including suggestions for reducing this burden, to Washington Headquarters Services, Directorate for Information Operations and Reports, 1215 Jefferson Davis Highway, Suite 1204, Arlington, VA 22202-4302, and to the Office of Management and Budget, Paperwork Reduction Project (0704-0188), Washington, DC 20503.

| | | | | |
|---|---|--|---|--|
| 1. AGENCY USE ONLY (Leave blank) | | 2. REPORT DATE November 1991 | 3. REPORT TYPE AND DATES COVERED Technical Memorandum | |
| 4. TITLE AND SUBTITLE Development of a Computer Algorithm for the Analysis of Variable-Frequency A.C. Drives - Case Studies Included | | | 5. FUNDING NUMBERS WU-946-02-2E | |
| 6. AUTHOR(S) M. David Kankam and Owen Benjamin | | | | |
| 7. PERFORMING ORGANIZATION NAME(S) AND ADDRESS(ES) National Aeronautics and Space Administration Lewis Research Center Cleveland, Ohio 44135-3191 | | | 8. PERFORMING ORGANIZATION REPORT NUMBER E-6688 | |
| 9. SPONSORING/MONITORING AGENCY NAMES(S) AND ADDRESS(ES) National Aeronautics and Space Administration Washington, D.C. 20546-0001 | | | 10. SPONSORING/MONITORING AGENCY REPORT NUMBER NASA TM-105327 | |
| 11. SUPPLEMENTARY NOTES M. David Kankam, NASA Lewis Research Center; Owen Benjamin, Cornell University, Ithaca, New York 14850 and 1991 Summer OAI/NASA Collaborative Aerospace Intern at Lewis Research Center. Responsible person, M. David Kankam, (216) 433-6143. | | | | |
| 12a. DISTRIBUTION/AVAILABILITY STATEMENT Unclassified - Unlimited Subject Category 07 | | | 12b. DISTRIBUTION CODE | |
| 13. ABSTRACT (Maximum 200 words) This report documents the development of a computer software for performance prediction and analysis of voltage-fed, variable-frequency AC drives for space power applications. The AC drives discussed include the pulse width modulated inverter (PWMI), the six-step inverter and the pulse density modulated inverter (PDMI), each individually connected to a wound-rotor induction motor. Various d-q transformation models of the induction motor are incorporated for user-selection of the most applicable model for the intended purpose. Simulation results of selected AC drives correlate satisfactorily with published results. Future additions to the algorithm are indicated in the Summary. These improvements should enhance the applicability of the computer program to the design and analysis of space power systems. | | | | |
| 14. SUBJECT TERMS Space power systems; Variable-frequency drives; Performance prediction; Computer software | | | 15. NUMBER OF PAGES 34 | |
| | | | 16. PRICE CODE A03 | |
| 17. SECURITY CLASSIFICATION OF REPORT Unclassified | 18. SECURITY CLASSIFICATION OF THIS PAGE Unclassified | 19. SECURITY CLASSIFICATION OF ABSTRACT Unclassified | 20. LIMITATION OF ABSTRACT | |



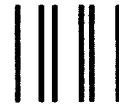
National Aeronautics and
Space Administration

Lewis Research Center
Cleveland, Ohio 44135

Official Business
Penalty for Private Use \$300

FOURTH CLASS MAIL

ADDRESS CORRECTION REQUESTED



Postage and Fees Paid
National Aeronautics and
Space Administration
NASA 451

NASA
